PCCP

PAPER

View Article Online
View Journal | View Issue

Cite this: *Phys. Chem. Chem. Phys.*, 2026, **28**, 8128

NMR methods for characterizing molecular species in two immiscible solvents: application to SABRE-hyperpolarised species

Guillaume Verhaeghe, Gaspard Huber and Patrick Berthault *

Received 18th December 2025,
Accepted 23rd February 2026

DOI: 10.1039/d5cp04938e

rsc.li/pccp

The potential of ^{1}H NMR for detecting solutes on either side of an interface between two immiscible liquids and studying their kinematic behavior is analysed. First, localised spectroscopy was used to monitor the migration of a solute from an aqueous phase to an organic phase and its self-diffusion coefficient was measured slice by slice within the two phases, validating the NMR approach. Next, a fast version of localised spectroscopy (Radsl-CSI) was designed and applied to track the migration of species hyperpolarised by parahydrogen from the organic phase where they are produced to the aqueous phase. This sequence evidenced the transfer of hyperpolarised pyridine from the organic phase to the aqueous phase.

Introduction

There are many situations where localised but detailed chemical information must be obtained quickly and NMR can be a valuable tool for obtaining such information. The study of hyperpolarised species obtained from optical pumping,[1] PHIP[2] or DNP[3] in solution is such a case, where the information needs to be extracted in a short time. Indeed, there is a need for fast identification of the molecular entities formed at the early stages of the dissolution or mixing, and in any case before the magnetisation returns to thermal equilibrium. Also, the case of chemical reactions requiring a liquid–liquid extraction (phase transfer) is such another situation where spatially resolved molecular information is highly valuable.[4]

Here, the focus is on SABRE[5] hyperpolarisation. As this process can be efficiently carried out only in an organic solvent such as methanol or dichloromethane, a key step is often to rapidly transfer the hyperpolarised species to an aqueous solvent. The sample thus becomes biphasic.

The potential of spatially resolved NMR has already been demonstrated in the field of organic chemistry to measure partition coefficients and study biphasic reaction kinetics.[6] However, in these cases, information from both phases is not acquired at the same time. The present work aims at assessing NMR methods for such a task. In this purpose, two model molecular systems are used.

Firstly, the evolution of a droplet of acetonitrile in a model biphasic system with deuterated water and deuterated dichloromethane (CD_2Cl_2, hereafter named DCM) after its introduction in the water phase is studied (Fig. 1). ACN has been chosen as it is soluble in both solvents; it does not give rise to a third phase. Secondly, dissolution of parahydrogen (pH_2) gas in a biphasic system containing D_2O and DCM (from top to bottom) with 25 mM pyridine and 5 mM IMes iridium catalyst as solutes is analysed. The first part of the study aims to develop NMR tools to study the phase transfer of a solute, with the aim of understanding and promoting the transfer of hyperpolarised species from the organic phase to the aqueous phase in the second part of the study.

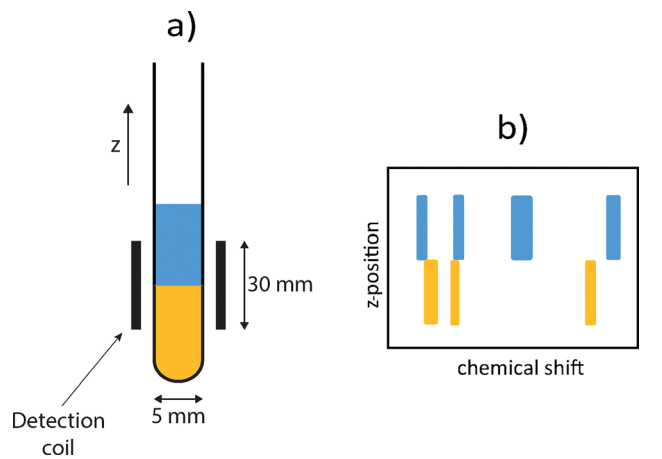

Fig. 1 (a) Biphasic solution in a 5 mm tube (blue: water phase and orange: dichloromethane). The interphase is placed at the middle of the radio-frequency coil. (b) Schematic view of the expected result: a series of ^{1}H spectra each giving the composition of the sample at a given *z*-position.

NIMBE, CEA, CNRS, Université de Paris-Saclay, CEA Saclay, 91191 Gif-sur-Yvette, France. E-mail: patrick.berthault@cea.fr

The specifications of such an approach include the experimental time and the spatial and spectral resolutions, which are related to sensitivity. The need to obtain this information along the whole sample simultaneously or at least on a short timescale compared to time constant evolution of the system, on the nuclear spins and chemical points of view, has also to be taken into account.

Materials and methods

Experimental conditions

The NMR experiments were performed on a Bruker Avance II 11.7 T (500 MHz ^{1}H) narrow-bore spectrometer equipped with a 5 mm broadband inverse probe head with three-axis gradients.

Migration and diffusion of ACN in a biphasic system CD_2Cl_2/D_2O. The sample was prepared in a 5 mm Shigemi tube (outer tube matching the magnetic susceptibility of $CDCl_3$, insert matching the susceptibility of D_2O). Such a tube was used in order to have the whole sample inside the detection coil region. The sample consisted of 200 μL of deuterated dichloromethane and 250 μL of heavy water. A solution of 0.96 M of ACN was prepared by adding 5 μL of pure ACN into 95 μL of D_2O. A drop of this solution was introduced on the top of the tube using a 10 μL micropipette. The solution slowly slid down the tube until gently reaching the top of the aqueous phase.

Hyperpolarisation of pyridine in a biphasic system CD_2Cl_2/D_2O. The sample was prepared in a 5 mm medium-wall NMR tube and consisted of 200 μL of each deuterated solvent. The DCM phase contained 25 mM of pyridine and 5 mM of IMes catalyst (iridium-based catalyst, IMes = 1,3-bis(2,4,6-trimethylphenyl)imidazole-2-ylidene), which was prepared by adding 0.64 mg of [IrCl(COD)(IMes)] (COD = cyclooctadiene) to 200 μL of CD_2Cl_2. The tube was then degassed before the addition of 4 bar of hydrogen gas. It was then shaken. The catalyst was left to activation overnight.[7] For the hyperpolarisation experiment, the gas phase of the tube was again removed before the addition of 4 bar of parahydrogen gas enriched at *ca.* 100%, using a homemade setup based on a 15 K cryostat which will be described elsewhere.

All the experiments described below were performed at 293 K.

In order to achieve spatial resolution in a short time, three NMR sequences were used in a comparative manner: OSDS,[8] LOCSY,[9] and tailored versions of CSI,[10] see Fig. 2. They are explained below.

NMR sequences

One-Shot Double Slice (OSDS). In OSDS,[8] the authors proposed to use the frequency-selective REBURP[11] pulse in an unusual way. While after proper calibration it performs on-resonance a perfect 180° flip of the magnetisation, according to its profile in the frequency domain, *xy*-magnetisation appears in the opposite phase between the effective offsets $+\Omega_{eff}$ and $-\Omega_{eff}$ (see simulation in Fig. S1 of the SI). When it is applied simultaneously with a *z* gradient along the tube axis (see Fig. 2a), the signals of the compounds that are in the upper solvent appear with a phase opposite to those from the lower solvent. This sequence allows one to have simultaneously the composition of both phases in a single 1D-spectrum. Nevertheless, two difficulties may arise. Firstly, due to the dephasing induced by the selective pulse with the application of a gradient, it is not possible to repeat the same experiment quickly. Secondly and more importantly, two compounds with the same chemical shifts but present in both solvents will lead to signal cancellation.

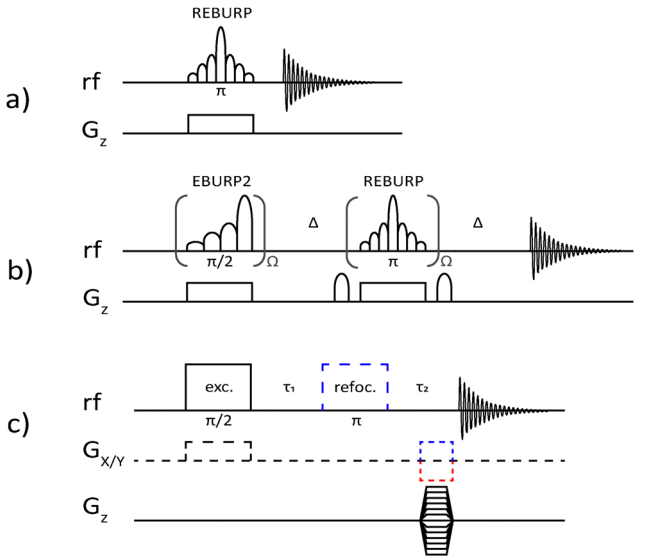

Fig. 2 Pulse sequences used. (a) OSDS and (b) LOCSY. The symbol Ω indicates a frequency offset incrementation. (c) CSI. For this last sequence, only a generic scheme is depicted, as different versions have been developed. For instance, the π refocussing pulse (refoc., dashed lines) transforms the gradient echo (red) into a spin echo (blue). Also, the excitation pulse (exc.) can be hard or frequency-selective simultaneous with a transverse gradient, according to the application. All CSI sequences use a phase gradient, represented on the G_Z row.

LOCalised SpectroscopY (LOCSY)

The second sequence has been proposed by Mantel *et al.* and is shown in Fig. 2b. LOCSY[9] consists of a spin echo, where the conventional (π/2)–(π) hard pulses are replaced, respectively, by excitation and refocussing frequency-selective pulses, applied simultaneously with a linear field gradient along the *z*-axis. Such pulses are defined with a bandwidth and a frequency offset that allows one to selectively excite a range of spin locations in the tube. By changing the pulse frequency offset, one can easily scan the tube in a discontinuous way. The strategy used by the authors in the original study was to obtain a set of 1D spectra and then stack them together in a 2D set. In this case, one cannot expect to obtain the information along the whole sample quickly. Therefore, we have slightly modified the approach. Instead, the strategy proposed here is to perform a 2D spectrum where the shaped pulses used for each point in the spatial dimension and their offsets are indicated in a list, for which a pointer is incremented between each row.

Moreover, a small interscan delay can be used because only the spins in the selected slice of the tube are excited.

At this stage, the spectrum will appear tilted due to chemical shift effects. This artefact arises from the fact that the frequencies are used at the same time for the spatial and the spectral encodings. Thus, if we consider the NMR spectrum of a compound located at a height z_c, the signals at opposite sides of this spectrum will appear in the slices slightly above and below z_c. An extra processing of the data, discussed in the original study, enables one to properly realign the spectrum thanks to a shearing transformation.

Chemical Shift Imaging (CSI)

Classical CSI with high spatial resolution. If the experimental time is not really a concern (as in the case of the slow migration of acetonitrile, see below), it can be interesting to use hard excitation and refocusing pulses in a spin-echo scheme (*i.e.*, hard π/2 and π-pulses, no slice gradient, and $\tau_1 = \tau_2$ in Fig. 2c). Thereby, a purely in-phase spectrum is obtained at the centre of the *k*-space (*i.e.*, when the phase gradient is null). This gives rise to sharper lines than when transformed in magnitude mode. The flip angle of the excitation pulse can be π/2 or – if the longitudinal relaxation time T_1 is known – the Ernst angle $\theta = \arccos(e^{-TR/T_1})$, with TR the interscan delay. The indirect (spatial) dimension can be linearly encoded (phase gradient evolution from $-G_{max}$ to $+G_{max}$ for instance).

3D CSI-DOSY experiment. It is possible to follow the CSI sequence block with a translational self-diffusion measurement. The pulse sequence and the Bruker pulse program as well as the experimental conditions, are given in Fig. S5 of the SI.

Fast CSI for hyperpolarised species. To obtain an efficient pulse sequence delivering the information in a short time, several tricks can be combined. The specifications adapted to hyperpolarised species are as follows: the number of radiofrequency pulses must be minimised, the sequence must be as fast as possible, and approximately the same amount of magnetisation must be present before each excitation. These considerations, as well as consideration of the cylindrical geometry of the NMR tube, led us to choose a longitudinal slice selection. Also, the choice of a radial evolution for the slice ensures both a similar volume and a minimal intersection between slices (see Fig. S2 of the SI). Note that the scheme is assumed to be less sensitive to convection effects[12] than a scheme with parallel longitudinal slices (which would suffer also from unequal slice volumes). From scan to scan, the slice gradient axis describes a radial trajectory in the *xy* plane (see the video on the repository site, and Fig. 3, with a soft pulse simultaneous to a varying transverse slice gradient). This ensures a minimal intersection of the slices, and thereby authorizes small interscan delays without magnetisation saturation. Fig. 3a displays the slices covered by such an approach, and Fig. 3b displays the time profile of the slice gradients in these CSI experiments. This approach has been preferred for the use of a hard pulse of incremented flip angle to compensate for the increasing incomplete longitudinal magnetisation recovery between scans.[13]

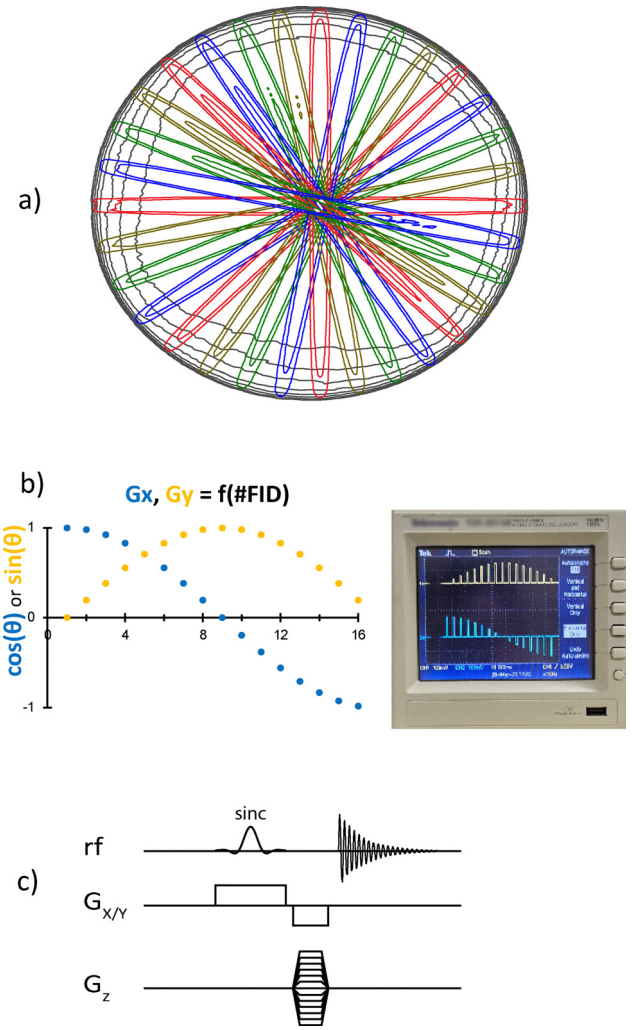

Fig. 3 Choice of the slices in the Radsl-CSI sequence. (a) Axial gradient-echo images of a water tube, without slice selection (whole circle) or with slice selection. (b) Time profile of the slice gradients in the Radsl-CSI experiments (left: expected and right: monitored with an oscilloscope connected after the gradient controller). (c) Pulse sequence used for Radsl-CSI.

Secondly, partial coverage of the *k*-space (phase gradient from 0 to $+G_{max}$) or centric encoding (phase gradient evolving as 0, $+\Delta G$, $-\Delta G$, $+2\Delta G$, $-2\Delta G$ *etc.*, with ΔG the gradient increment) can be used, the latter being more beneficial. In any case, for this unbalanced state of hyperpolarisation (altered by relaxation and radiofrequency pulses), it is important to first use maximum magnetization at the beginning of the sequence to encode the points at the centre of the reciprocal space where the gradients are the weakest.[14] At worst, the decrease in polarisation will lead to a slight blurring effect in the spatial dimension of the experiment. It is noted that, in the case of centric encoding, the processing cannot consist in a double Fourier transformation; rather the data must be reordered in the indirect dimension before they are Fourier transformed. A home-made python has been written in this purpose.

Finally, a gradient-echo scheme is preferred for hyperpolarised species (no refocusing pulse and $\tau_1 = 0$), as (i) it is

Table 1 Comparison of the four pulse sequences used

Sequence	OSDS	LOCSY	CSI	Radsl-CSI
Need for *xyz* gradients	N	N	N	Y
Type of Fourier transformation	1D	1D	2D	2D
Simultaneous information	Y	N	Y	Y
Spatial resolution	–	+	+	+
Spectral discrimination	+ –	+ + +	+ + +	+ + +
Phase-sensitive spectra	Y	Y	Y	N
Speed	+ + +	+ +	+	+ +

sometimes difficult to invert intense polarisation[15] and (ii) the rf coil not covering the whole solution could lead to a mixture of up and down magnetisation.

Fig. 3c depicts the final pulse sequence used for this accelerated experiment that has been denoted as Radsl-CSI for Radial-slice CSI. The Bruker pulse sequence is given in the SI, Fig. S10.

Table 1 shows the comparison of the four pulse sequences that have their own advantages and disadvantages. Considering the speed criterion, OSDS only needs one scan and is therefore the fastest. However, it provides only very rudimentary spatial localisation (positively phased signals for nuclei in one solvent and negatively phased signals for nuclei in the other). Now considering the simultaneity criterion, CSI and derivatives are the only sequences providing the observation of the whole sample at the same time. In contrast, LOCSY works by acquiring the signal slice after slice in a discontinuous manner. Nevertheless, it could be advantageous to use this sequence to observe what is happening at a specific location in the sample through the time, like a camera. It is noted that, among all these sequences, Radsl-CSI is the only one that, for reasons of speed related to optimized slice selection, requires the use of 3-axis gradients, which is not available on all commercial probes.

Data processing

Home-built python programs have been developed to process the NMR data (available on the repository site). The NMRGLUE package[16] was used for reading and writing data in the Bruker format.

Results

Migration of acetonitrile in a biphasic solution

10 μL of acetonitrile (ACN) at 0.96 M in D_2O were introduced on top of the NMR tube containing the deuterated solvents. The excess of water compared to DCM allowed the edge of the sample to be slightly above the NMR coil, which gave time to observe the beginning of the migration of ACN. The experiment was monitored using the CSI sequence, and consisted of 64 FIDs in the spatial dimension, each of them recorded with 4 transients. The duration of each experiment was 8 min 33 s and the migration was observed for 40 hours.

Fig. 4a displays three of these CSI contour plots, evidencing the progression of ACN first through the aqueous phase and then into the organic phase. On these maps, in the direct (spectral) dimension from left (low field) to right, the signals

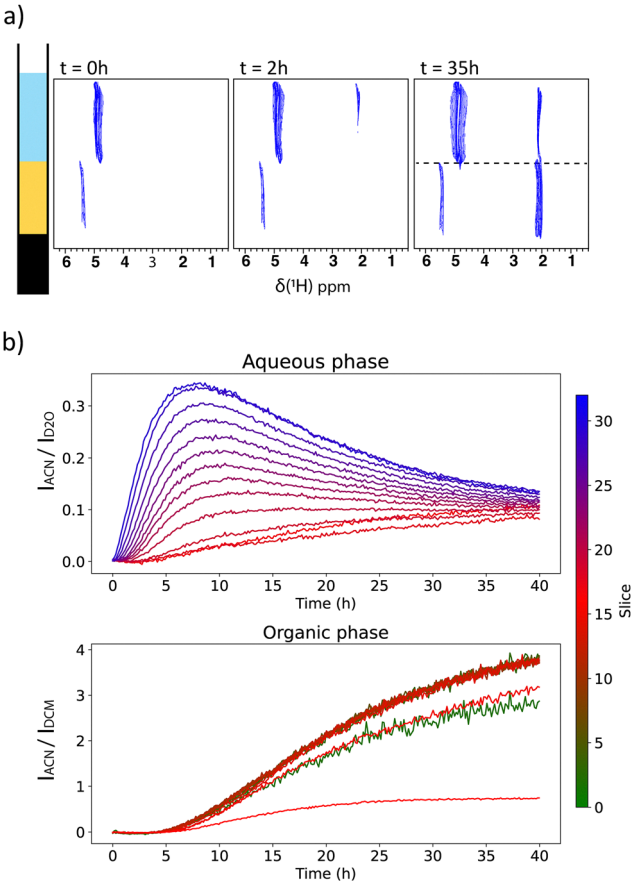

Fig. 4 Time evolution of CSI experiments after introduction of a droplet of acetonitrile on top of the biphasic solution. (a) Three CSI contour plots taken at different moments after the introduction of the solute. (b) Time evolution of the ACN signal in each slice of the water phase (top) and the dichloromethane phase (bottom). For clarity, the slices have been grouped in pairs and their colour reflects the location of the slice in the *z* dimension based on the vertical scale bar.

are those of dichloromethane (residual $CHDCl_2$, 5.3 ppm), water (residual HDO, 4.8 ppm) and acetonitrile (2.1 ppm), respectively. The more intense water signal is due to a more elevated water content of the added acetonitrile droplet. The rupture linked to the interface is well visible on the contour plots. The curves in Fig. 4b give the evolution of the ACN normalised signal intensity in each sample slice (in the organic phase, at the top, and in the water phase, at the bottom). Regarding the aqueous phase, the behaviour of acetonitrile varies depending on the position of the slice. Far from the interface, we can clearly see the acetonitrile drop arriving, reaching a maximum. Then the signal decreases, and the ACN concentration eventually becomes uniform across all slices of this phase. For each slice, the following piecewise model built with exponential curves could satisfactorily fit the time evolution of the ACN signal (six variables):

- For $t \leq t_{up}$: $S(t) = 0$
- For $t_{up} < t \leq t_{down}$: $S(t) = I_{max}\left(1 - e^{-k_{up}(t-t_{up})}\right)$
- For $t_{down} < t$: $S(t) = \left(I_{max}\left(1 - e^{-k_{up}(t_{down}-t_{up})} - I_{inf}\right)e^{-k_{down}(t-t_{down})} + I_{inf}\right)$

where k_{up} corresponds to the rate of appearance of ACN in the

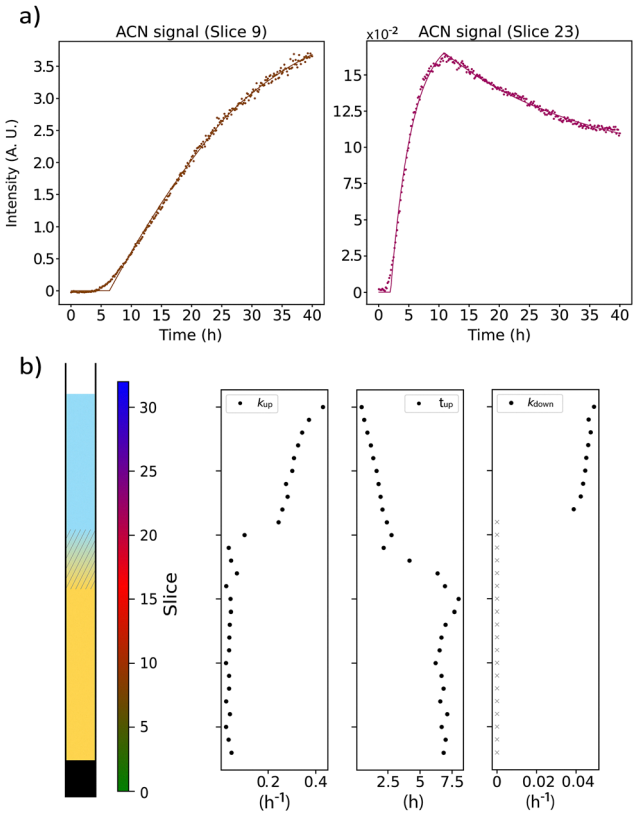

Fig. 5 Evolution of the ACN signal and fit using the exponential model. (a) Two slices taken in each phase (left: DCM and right: water). (b) Parameters k_{up}, t_{up} and k_{down} extracted from the fit for each slice of the tube. It is noted that the values of k_{down} in dichloromethane are set to 0 and displayed in light grey because they have no meaning.

considered slice, k_{down} represents the rate of disappearance, t_{up} is the time at which the curve deviates from the baseline, and t_{down}, when not at the limit, is the time of change in the curve's behaviour. I_{max}, in DCM, and I_{inf} represent the normalised intensities at equilibrium, and should be related to the partition coefficient. For consistency, we used the same equation to fit the curves in both phases, but note that the evolution of the ACN signal in the organic phase could be modelled with a single-delayed exponential (t_{down} joining the long-time limit).

All the curves and the associated fits are displayed in the SI (Fig. S3 and S4).

Fig. 5a shows one of these fits for each phase, and Fig. 5b displays the k_{up}, t_{up} and k_{down} values for each slice of the sample.

Dealing with t_{up} (graph at the middle), in the aqueous phase, this delay of ACN appearance increases when approaching the interface, which can be explained by the very slow progression of the solute in water; conversely, as soon as the interface is crossed, the solute is instantly observed in all slices of the dichloromethane phase. By the way note that the velocity k_{up} is approximately identical across all slices of the dichloromethane phase (excluding the interface and the edge of the tube), whereas in the aqueous phase the k_{up} values decrease when approaching the interface (appearance of ACN in the slices close to the interface compensated by loss to the organic phase). It is noted that simultaneously the k_{down} values decrease when approaching the interface, however with a lower slope.

On a similar sample, after equilibration of the species in solution, a localised-DOSY experiment was undertaken. In this purpose, the spin-echo CSI sequence was followed by a stimulated echo diffusion-encoded sequence using bipolar gradients (pulse sequence in the SI, Fig. S5). The purpose of such a sequence is to obtain information on the diffusivity of molecules at different locations within the sample. Other spatially localized sequences providing access to this type of information already exist in the literature, whether it be the basic sequence for monitoring electrolytes in a lithium-ion battery,[17] diffusion-weighted spectroscopic MRI,[18] or the more sophisticated SMOOSY sequence,[19] among others. The diffusion gradients were applied along y, in order to minimize potential deleterious convection effects. Fig. 6 displays the signal intensities and extracted self-diffusion coefficients of (a) dichloromethane, (b) water and (c) acetonitrile for each slice of the sample (details of each diffusion curve for ACN are given in Fig. S6 and S7 of the SI). The intensities exhibit a rather flat profile along the tube for a given phase, proving the quality of the CSI part. Note that the intensity profile seems to be not null for dichloromethane in the water phase, which is actually an artefact. It is only due to the shoulder of the water peak that overlaps the dichloromethane resonance frequency.

Initially, such an experiment gave a surprising result: while the intensity profiles appeared rather flat, the diffusion coefficients seemed to significantly increase from the edge of the solution to the interface (up to a factor of 2 for instance for acetonitrile, see Fig. S8c of the SI). We assumed that this could be due to a non-uniformity of the y gradient amplitude along z, as these gradients on a high-resolution probe head are only designed for coherence selection.

This issue has already been addressed in the literature,[20] but here in order to correct the non-uniformity of the y-gradient along z, a calibration of its real value against the z-location was performed. In this purpose, for each z-slice of a 5 mm outer diameter tube filled with water, the frequency spreading of the signal was monitored when increasing the nominal gradient strength (g). Thus, each local gradient strength could be calculated considering the full width at half maximum, denoted as $\Delta\nu$, and the inner diameter of the tube, denoted d:

$$G_{calc}(z,g) = \frac{\Delta\nu}{\gamma d}$$

The diffusion profiles before this correction, the exact calibration method and the results of this calibration are given in Fig. S8 of the SI, and Fig. 6 displays the diffusion profiles after correction.

After such correction, the transverse diffusion profiles are rather flat. The mean self-diffusion values are found to be $D_{D_2O} = (1.91 \pm 0.01) \times 10^{-9}$ m^2 s^{-1} (18 points) and $D_{DCM} = (3.76 \pm 0.01) \times 10^{-9}$ m^2 s^{-1} (22 points), in accordance with the literature.[21,22]

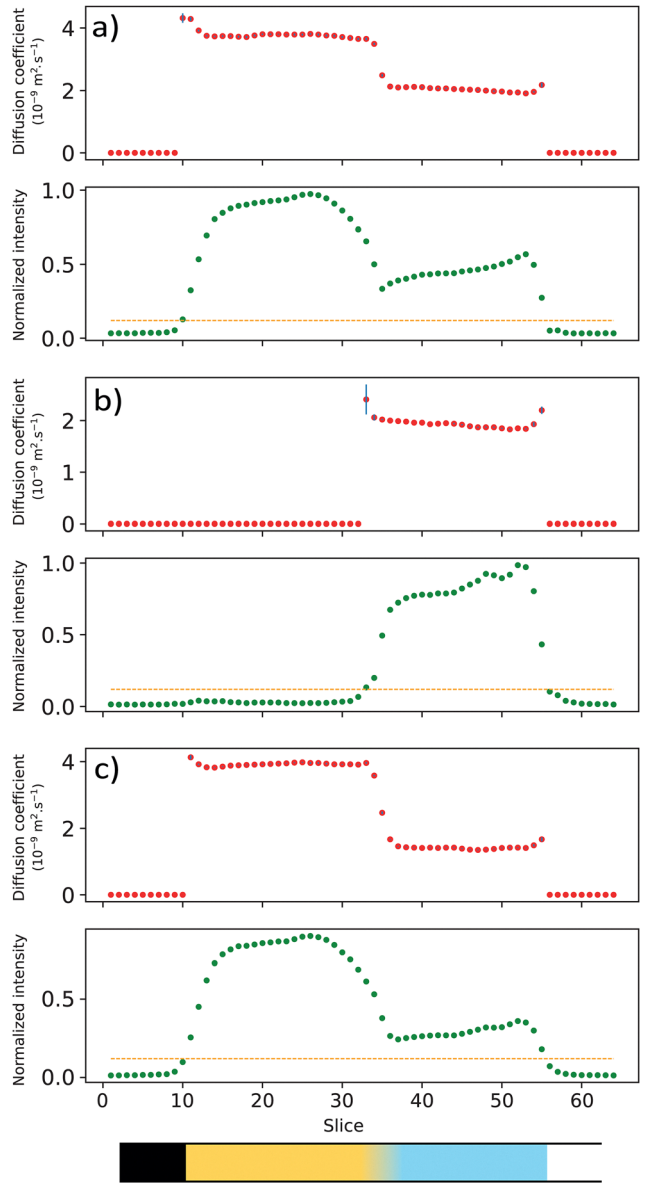

Fig. 6 Results of the CSI-DOSY experiments: normalized signal intensity (green) and diffusion coefficient (red) for (a) DCM, (b) water, and (c) ACN, in the different *z* slices of the sample. The dashed yellow lines represent the threshold below which the diffusion coefficients have not been estimated.

The self-diffusion coefficient profile of acetonitrile follows that of the solvent in which it is. A sudden increase is observed when passing from the water phase ($D_{ACN} = (1.41 \pm 0.01) \times 10^{-9}$ m^2 s^{-1} (18 points)) to the DCM phase ($D_{ACN} = (3.93 \pm 0.01) \times 10^{-9}$ m^2 s^{-1} (22 points)). At the exact location of the interface, the error bar on the extracted diffusion coefficient was high, probably due to the presence of a meniscus between the two solutions. The increase of the ACN diffusion coefficient between the aqueous and the DCM phase correlates with the appearance of its NMR signal in all organic slices during the migration experiment.

Some authors mentioned an accelerated lateral diffusion of solutes near the interface.[23] In this study, we were unable to detect such an effect.

Hyperpolarisation transfer from the organic to the aqueous phase

Finally, the accelerated version of the CSI experiment (mentioned above as Radsl-CSI) with centric encoding was used with species hyperpolarised by the SABRE method. The same biphasic water/dichloromethane system was used, but this time the organic phase contained 5 mM IMes catalyst (previously activated) and 25 mM pyridine. Four bars of parahydrogen gas enriched at *ca.* 100% were introduced in the tube, which was then vigorously shaken in a magnetic field of *ca.* 6.5 mT during 15 s before being introduced in the spectrometer magnet. Immediately, a Radsl-CSI sequence was run, for an experiment time of 7 seconds.

Fig. 7 compares the low field part of the contour plots obtained (a) just after the introduction of the tube in the

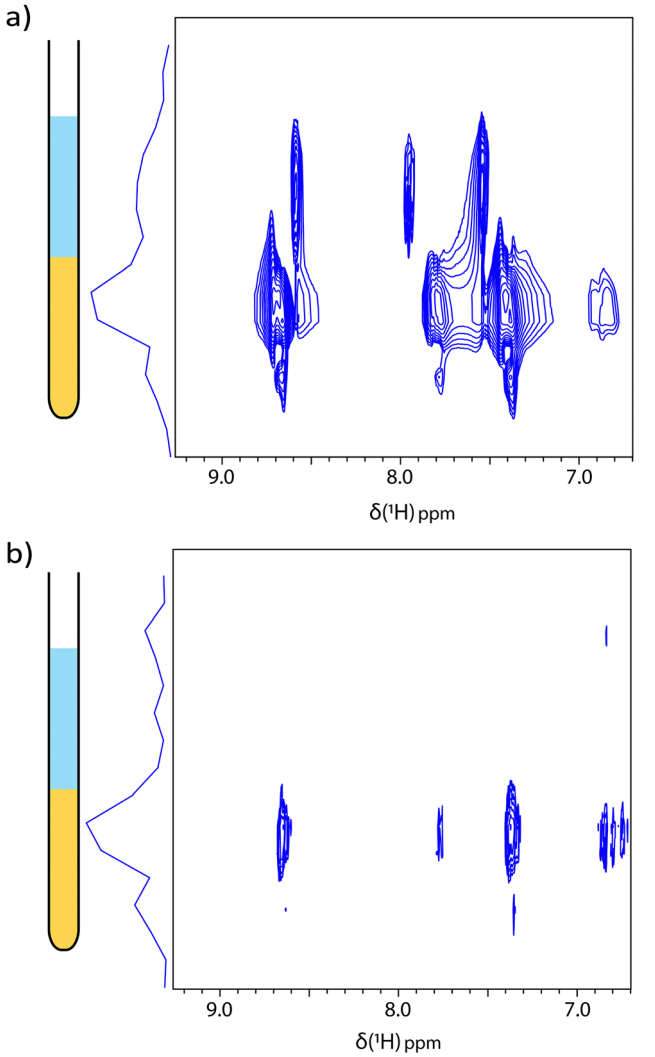

Fig. 7 Results of the Radsl-CSI experiments: ^{1}H contour plots showing the aromatic region (magnitude mode). From left to right, the signals are those of *ortho*-pyridine (around 8.6 ppm), *para*-pyridine (around 7.9 ppm), and *meta*-pyridine (around 7.4 ppm). The signals on the rightest part of the spectra are those of the catalyst. (a) Hyperpolarised and (b) thermal spectra. The duration of each experiment was *ca.* 8 seconds.

spectrometer magnet, after 15 s of shaking, and (b) two minutes later when hyperpolarisation is gone. The same acquisition and processing parameters have been applied for each experiment, and the same levels are displayed for both contour plots. Fig. S9 of the SI shows spectra of highest intensity in the organic phase and aqueous phase extracted from these contour plots.

Not only is the signal-to-noise ratio gain significance in dichloromethane (up to 73 for the meta proton of the pyridine), but also signals from hyperpolarised pyridine in the aqueous phase can be clearly distinguished. Due to the lack of pyridine signal in the spectra of the water phase at thermal equilibrium, the signal enhancement could not be accurately estimated. In the hyperpolarised spectra, their narrow line width and frequency shift indicate that these are not dichloromethane bubbles in water, but rather a phase transfer of the solute after hyperpolarisation (since the IMes catalyst is mainly soluble in dichloromethane and dihydrogen is also more soluble in dichloromethane, hyperpolarisation could only occur in the organic phase). Note the similitude between the spatial profiles for the organic phase in the hyperpolarised and thermal spectra (vertical projections in Fig. 7a and b, respectively), which proves that their non-flat profile is only due to the pulse sequence (not enough points acquired in this dimension to obtain a flat profile). To flatten this profile by attenuating this effect linked to a too small number of sampled points, one could normalise with a reference spectrum or correct with a spatial filtering[24] (the inverse Hamming function for instance) before Fourier transformation.

Optimization of the extraction step of hyperpolarised molecular species toward the aqueous phase after the SABRE experiment can be achieved in several ways, most of which are chemical in nature. In the CASH-SABRE approach, Iali *et al.*[25] described the use of salts – mainly NaCl – to accelerate the transfer of the hyperpolarised species to the aqueous phase. To go a step further toward the acceleration of this step, exploitation of the salting-in effect based on the use of anions and cations adequately chosen in the Hofmeister series[26] should be an interesting avenue. It is currently being pursued in our laboratory.

Conclusions and outlook

The present work focused on the implementation of NMR sequences enabling the localisation of molecular species in solution. The proposed methods constitute robust tools for more easily understanding the behaviour of molecular species in a multiphase system, such as determining the partition coefficient, measuring the rate of transfer as a function of experimental conditions, and calculating the self-diffusion coefficient.

The sequences presented here form the basis for more sophisticated localised sequences, such as the localised DOSY experiment, which is of high interest.[27] But it could also be any kind of NMR scheme, such as COSY, TOCSY, or NOESY, if coherence selection is ensured *via* phase cycling or field gradients.

The CSI-DOSY sequence will be tested on other model biphasic systems, and completed by the (i) change of the experimental conditions, (ii) variation of several NMR parameters such as the direction of the diffusion-encoding gradients and the probed diffusion length, and (iii) use of motion models. Also, other sequences such as those involving interphase transfer of magnetisation[28] will be investigated.

The newly conceived Radsl-CSI sequence has enabled the observation of a hyperpolarised solute transferred from the organic phase, where hyperpolarisation occurs, to the aqueous phase, where it was detected. For the fate of hyperpolarised molecular species after the SABRE experiment, the path we are now interested in involves chemical modifications of the solutions in order to (i) accelerate the phase separation that occurs just after the shaking and (ii) increase the solubility of compounds of interest in the aqueous phase.

Author contributions

Guillaume Verhaeghe: investigation, methodology, writing – original draft, and writing – review and editing. Gaspard Huber: investigation and writing – review and editing. Patrick Berthault: conceptualization, investigation, methodology, writing – original draft, and writing – review and editing.

Conflicts of interest

There are no conflicts to declare.

Data availability

After publication, the data (NMR raw and processed data) will be posted on the national Recherche Data Gouv website (https://recherche.data.gouv.fr/fr/page/entrepot-recherche-data-gouv) and made available to anyone who wishes to access it. See DOI: https://doi.org/10.57745/CQ6LUC.

Supplementary information (SI): time-resolved CSI experiments; CSI-DOSY pulse sequences; self-diffusion curves; details of the gradient calibration; pulse sequences of the Radsl-CSI experiment; localised ^{1}H spectra recorded with and without hyperpolarisation. See DOI: https://doi.org/10.1039/d5cp04938e.

Acknowledgements

Support from the French Ministry of Research (projects ANR-23-CE29-0013-03 SOFTNMR and ANR-25-CE29-5590-03 STEREOMAG) is acknowledged.

Notes and references

1 P. Berthault, A. Bogaert-Buchmann, H. Desvaux, G. Huber and Y. Boulard, Sensitivity and Multiplexing Capabilities of MRI Based on Polarized ^{129}Xe Biosensors, *J. Am. Chem. Soc.*, 2008, **130**, 16456–16457.

2 B. J. Tickner and V. V. Zhivonitko, Advancing homogeneous catalysis for parahydrogen-derived hyperpolarisation and its NMR applications, *Chem. Sci.*, 2022, **13**, 4670–4696.
3 K. Dos Santos, G. Bertho, C. Caradeuc, V. Baud, A. Montagne, D. Abergel, N. Giraud and M. Baudin, A Toolbox for Glutamine Use in Dissolution Dynamic Nuclear Polarization: from Enzymatic Reaction Monitoring to the Study of Cellular Metabolic Pathways and Imaging, *Chem. Phys. Chem.*, 2023, **24**, e202300151.
4 J. A. Almohasin, J. Balag, V. G. Miral, R. V. Moreno, L. J. Tongco and E. C. R. Lopez, Green solvents for liquid–liquid extraction: recent advances and future trends, *Eng. Proc*, 2023, **56**, 174.
5 R. W. Adams, J. A. Aguilar, K. D. Atkinson, M. J. Cowley, P. I. P. Elliott, S. B. Duckett, G. G. R. Green, I. G. Khazal, J. López-Serrano and D. C. Williamson, Reversible interactions with *para*-hydrogen enhance NMR sensitivity by polarization transfer, *Science*, 2009, **323**, 1708–1711.
6 Y. Ben-Tal and J. E. Hein, Slice-selective NMR for quantitative analysis of liquid–liquid biphasic systems: a tool for organic chemists, *J. Org. Chem.*, 2025, **90**, 7832–7840.
7 L. S. Lloyd, Developing SABRE as an analytical tool in NMR, PhD thesis, University of York, 2013.
8 K. D. Catlin, J. Simmons and S. Bai, A one-shot double-slice selection NMR method for biphasic systems, *Phys. Chem. Chem. Phys.*, 2022, **24**, 17961–17965.
9 C. Mantel, P.-A. Bayle, S. Hediger, C. Berthon and M. Bardet, Study of liquid–liquid interfaces by an easily implemented localized NMR sequence, *Magn. Reson. Chem.*, 2010, **48**, 600–606.
10 T. R. Brown, B. M. Kincaid and K. Ugurbil, NMR chemical shift imaging in three dimensions, *Proc. Natl. Acad. Sci. U. S. A.*, 1982, **79**, 3523–3526.
11 H. Geen and R. Freeman, Band-selective radiofrequency pulses, *J. Magn. Reson.*, 1991, **93**, 93–141.
12 I. Swan, M. Reid, P. W. A. Howe, M. A. Connell, M. Nilsson, M. A. Moore and G. A. Morris, Sample convection in liquid-state NMR: why it is always with us, and what we can do about it, *J. Magn. Reson.*, 2015, **252**, 120–129.
13 A. V. Ouriadov, W. W. Lam and G. E. Santyr, Rapid 3-D mapping of hyperpolarized ^{3}He spin-lattice relaxation times using variable flip angle gradient echo imaging with application to alveolar oxygen partial pressure measurement in rat lungs, *Magn. Reson. Mater. Phys., Biol. Med.*, 2009, **22**, 309–318.
14 G. J. Topping, C. Hundshammer, L. Nagel, M. Grashei, M. Aigner, J. G. Skinner, R. F. Schulte and F. Schilling, Acquisition strategies for spatially resolved magnetic resonance detection of hyperpolarized nuclei, *Magn. Reson. Mater. Phys., Biol. Med.*, 2020, **33**, 221–256.
15 P. Berthault, H. Desvaux, G. Le Goff and M. Pétro, A simple way to properly invert intense nuclear magnetization: application to laser-polarized xenon, *Chem. Phys. Lett.*, 1999, **314**, 52–56.
16 J. J. Helmus and C. P. Jaroniec, Nmrglue: an open source Python package for the analysis of multidimensional NMR data, *J. Biomol. NMR*, 2013, **55**, 355–367.
17 S. A. Krachkovskiy, J. D. Bazak, P. Werhun, B. J. Balcom, I. C. Halalay and G. R. Goward, Visualization of Steady-State Ionic Concentration Profiles Formed in Electrolytes during Li-Ion Battery Operation and Determination of Mass-Transport Properties by *in Situ* Magnetic Resonance Imaging, *J. Am. Chem. Soc.*, 2016, **138**, 7992–7999.
18 I. Ronen and J. Valette, in *eMagRes*, eds. R. K. Harris and R. L. Wasylishen, John Wiley & Sons, Ltd, Chichester, UK, 2015, pp. 733–750.
19 K. Ito, Y. Tsuboi and J. Kikuchi, Spatial molecular-dynamically ordered NMR spectroscopy of intact bodies and heterogeneous systems, *Commun. Chem.*, 2020, **3**, 80.
20 M. A. Connell, P. J. Bowyer, P. Adam Bone, A. L. Davis, A. G. Swanson, M. Nilsson and G. A. Morris, Improving the accuracy of pulsed field gradient NMR diffusion experiments: correction for gradient non-uniformity, *J. Magn. Reson.*, 2009, **198**, 121–131.
21 D. E. O'Reilly, E. M. Peterson and E. L. Yasaitis, Self-diffusion coefficients and rotational correlation times in polar liquids. IV. Dichloromethane and pyridine, *J. Chem. Phys.*, 1972, **57**, 890–894.
22 H. Kato, T. Saito, M. Nabeshima, K. Shimada and S. Kinugasa, Assessment of diffusion coefficients of general solvents by PFG-NMR: investigation of the sources error, *J. Magn. Reson.*, 2006, **180**, 266–273.
23 J. B. Buhn, P. A. Bopp and M. J. Hampe, A molecular dynamics study of a liquid–liquid interface: structure and dynamics, *Fluid Phase Equilib.*, 2004, **224**, 221–230.
24 M. S. Hansen and P. Kellman, Image reconstruction: an overview for clinicians, *J. Magn. Reson. Imaging*, 2015, **41**, 573–585.
25 W. Iali, A. M. Olaru, G. G. R. Green and S. B. Duckett, Achieving high levels of NMR-hyperpolarization in aqueous media with minimal catalyst contamination using SABRE, *Chem. – Eur. J.*, 2017, **23**, 10491–10495.
26 Y. Marcus, Effect of ions on the structure of water: structure making and breaking, *Chem. Rev.*, 2009, **109**, 1346–1370.
27 T. Koev, H. Hussain, K. Gukhool and M. Wallace, Spatially resolved diffusion NMR for structurally heterogeneous materials, *ChemRxiv*, 2025, preprint, DOI: 10.26434/chemrxiv-2025-7x86l.
28 R. Nepravishta, S. Monaco, J. C. Muñoz-García, Y. Z. Khimyak and J. Angulo, Spatially resolved STD-NMR applied to the study of solute transport in biphasic systems: application to protein–ligand interactions, *Nat. Prod. Commun.*, 2019, **14**, 1934578X19849789.